

European Journal of Applied Mathematics

<http://journals.cambridge.org/EJM>

Additional services for *European Journal of Applied Mathematics*:

Email alerts: [Click here](#)

Subscriptions: [Click here](#)

Commercial reprints: [Click here](#)

Terms of use : [Click here](#)



Mean curvature flow by the Allen–Cahn equation

D. S. LEE and J. S. KIM

European Journal of Applied Mathematics / Volume 26 / Issue 04 / August 2015, pp 535 - 559
DOI: 10.1017/S0956792515000200, Published online: 13 May 2015

Link to this article: http://journals.cambridge.org/abstract_S0956792515000200

How to cite this article:

D. S. LEE and J. S. KIM (2015). Mean curvature flow by the Allen–Cahn equation. *European Journal of Applied Mathematics*, 26, pp 535-559 doi:10.1017/S0956792515000200

Request Permissions : [Click here](#)

Mean curvature flow by the Allen–Cahn equation

D. S. LEE¹ and J. S. KIM²

¹*Department of Mathematical Sciences, Ulsan National Institute of Science and Technology, Ulsan 689-798, Republic of Korea*

²*Department of Mathematics, Korea University, Seoul 136-713, Republic of Korea
email: esen@unist.ac.kr, cfdkim@korea.ac.kr*

(Received 4 April 2014; revised 12 April 2015; accepted 13 April 2015; first published online 13 May 2015)

In this paper, we investigate motion by mean curvature using the Allen–Cahn (AC) equation in two and three space dimensions. We use an unconditionally stable hybrid numerical scheme to solve the equation. Numerical experiments demonstrate that we can use the AC equation for applications to motion by mean curvature. We also study the curve-shortening flow with a prescribed contact angle condition.

Key words: motion by mean curvature, Allen-Cahn equation, contact angle condition

1 Introduction

We study the evolution of curves and surfaces under the mean curvature flow by using the AC equation [1]:

$$\phi_t(\mathbf{x}, t) = -\frac{F'(\phi(\mathbf{x}, t))}{\epsilon^2} + \Delta\phi(\mathbf{x}, t), \quad \mathbf{x} \in \Omega, \quad t > 0, \quad (1.1)$$

where $\Omega \subset \mathbb{R}^d$ ($d = 2, 3$) is a domain. The AC equation is originally introduced to describe motion of the interfaces in materials. Here, the phase-field ϕ is a non-conserved order parameter. The function $F(\phi) = 0.25(\phi^2 - 1)^2$ is the Helmholtz free-energy functional. The small constant ϵ is the gradient energy coefficient related to the interfacial energy. In this paper, we study the AC equation with and without the contact angle boundary conditions.

The study of free boundary problems can be separated into two groups: diffuse-interface problems and geometric evolutionary problems [18]. A typical diffuse-interface description of an antiphase domain wall motion is well established by using the AC equation [1]. This equation is also known that it corresponds to the mean curvature flow as the geometric evolution equation [17, 32, 72–74].

Let us first consider the mean curvature flow in the field of differential geometry. We can define that a family of surfaces $\{M\}$ in \mathbb{R}^d is said to be moving by mean curvature provided that

$$\frac{\partial \mathbf{x}}{\partial t} = H(\mathbf{x}, t)\mathbf{n}(\mathbf{x}, t), \quad \mathbf{x} \in M, \quad 0 < t,$$

where $H(\mathbf{x}, t)$ and $\mathbf{n}(\mathbf{x}, t)$ denote mean curvature and outer normal of the surface M at (\mathbf{x}, t) . Namely, normal velocity of the surface simply equals its mean curvature.

From a different point of view, motion by mean curvature can be considered as the singular limit of the AC equation. The AC model, based on the Ginzburg–Landau theory, is used to describe microstructure phenomena. It describes a microstructure using non-conserved order parameter ϕ . This parameter takes distinct constant values in each of the coexisting ordered states and varies smoothly across the interface between two different states. The interface then can be represented as the zero level-set of the order parameter. For this reason, the AC equation is often referred to as the diffuse-interface model. One of the properties of the AC equation is that the zero level solution converges to the mean curvature flow. Thus, the interfacial region between two different regions ± 1 evolves by the mean curvature flow. In this paper, we consider the solution of the AC equation as the diffuse-interface model, and compare with the geometric evolution equation.

Many of the previous works have studied the mean curvature flow on developing numerical schemes. In front tracking method, Barrett, Garcke and Nürnberg proposed the parametric finite element approximation of geometric curve evolutions for curve networks and anisotropic surface [11] and surface clusters [9]. They also studied the coupled surface and grain boundary motion in bi- and tricrystals in [10]. As an application for BMO algorithm [60], Ruuth and his collaborators developed the diffusion-generated methods for multiple grains [68].

On the application of the geometric flow, Mullins [62] initially proposed the mean curvature flow to model the formation of grain boundaries in annealing metals. Gurtin [46] derived the mean curvature flow as a model for motion of the interface, and Angenent and Gurtin [3] developed motion for perfect conducts. The AC equation is used for a phase-field model that approximates motion by mean curvature [1, 20, 61].

In addition, the sharp-interface limit of the gradient flow dynamics was investigated in [8, 32, 73, 74], and interface area and interface curvature problems were studied by [66]. There were also level-set formulations of viscosity solutions for hypersurfaces by Chen *et al.* [21] and a geometrical approach [7]. Independently, Evans and Spruck [33–36], and Soner [72] also introduced motion by level-set methods. Ilmanen [52] showed that this limit is actually one of the Brakke’s motions [16] by the mean curvature solution. In the radial symmetric case, Bronsard and Kohn [17] derived that, as $\epsilon \rightarrow 0$, the zero level-set of ϕ approaches a surface, which moves with a normal velocity equal to the mean curvature of the surface. On the one hand, the pioneering geometric works for the curve-shortening flow were done by Tso [75], Gage and Hamilton [40], and Grayson [42]. Further details can be found in [29, 31, 44] and references therein. The hypersurfaces of higher codimension where we assign its velocity vector by mean curvature vector to form the more than codimension 1, is not well known about singularities. Recently, higher codimension for the mean curvature flow has also received attention [2, 4, 19, 71], and on the other hand, the solution of the AC equation has been considered for De Giorgi’s conjecture [41, 64]. As for the curvature driven flow, there are also a lot of applications for the anisotropic mean curvature flow [14], image process [30, 57, 69], phase separation and damage [48], grain boundary motion [63], fluid dynamics [37], pulsating wave [27] and smoothing triangular surface [77].

Various numerical methods have been applied to illustrate the motion by mean curvature. Among them are level set methods [23–25, 47], finite element methods [11, 12, 26, 28, 38, 39], and Delaunay tessellations [15]. But there is no geometric verification or numerical evidence for phase-field methods in terms of motion by mean curvature. Applying the stable and hybrid scheme [56], we confirm that numerical experiments give good agreements with geometrical results under the mean curvature flow.

Here, we describe how the algorithm works from numerical aspects, and show some numerical simulations including two- and three-dimensional cases. Since the family of solutions whose zero level sets of the AC equation follows the mean curvature flow, the validity of the numerical algorithm can be demonstrated by its geometric evolution equation. Thus, the results of numerical experiments with and without the prescribed contact angle boundary condition verify theoretical understanding under the mean curvature flow. The main content is divided in four parts. In Section 2, we discuss the mean curvature flow driven by the AC equation. An unconditionally stable hybrid numerical method for the AC equation is described in Section 3. Examples and numerical tests for closed curves are given in Section 4. We consider a planar curve having end-points moving freely along a boundary with prescribed contact angles in Section 5. In summary, Section 6 concludes with a discussion of test results.

2 Allen–Cahn equation for motion by mean curvature

It is known that in the limit of small ϵ the zero level solution reduces to motion by mean curvature of the interface between the stable ± 1 phases [1, 32, 67]. We briefly show that the interface moves with normal velocity proportional to their mean curvature. We design a new coordinate in the neighbourhoods of the surface $\phi = 0$. Let us define $r = r(x, y, z, t)$ as the signed distance of (x, y, z) from $\phi = 0$, where $r < 0$, if $\phi(x, y, z, t) > 0$ and $r > 0$, if $\phi(x, y, z, t) < 0$. First, we denote the outer unit normal to the surface by $\mathbf{n} = \nabla\phi/|\nabla\phi|$. Then, it deduces $\mathbf{n} \cdot \mathbf{n} = 1$ and $\mathbf{n} \cdot \mathbf{n}_r = 0$, where \mathbf{n}_r is the rate of change of \mathbf{n} in the direction of r coordinate, (see Figure 1).

Now the term $\Delta\phi$ can be rewritten as follows:

$$\begin{aligned} \Delta\phi &= \nabla \cdot \nabla\phi = \nabla \cdot (|\nabla\phi|\mathbf{n}) = \nabla \cdot ((\nabla\phi \cdot \mathbf{n})\mathbf{n}) = \nabla \cdot (-\phi_r\mathbf{n}) \\ &= -\nabla\phi_r \cdot \mathbf{n} - \phi_r\nabla \cdot \mathbf{n} = -(\nabla\phi)_r \cdot \mathbf{n} - \phi_r\nabla \cdot \mathbf{n} = (\phi_r\mathbf{n})_r \cdot \mathbf{n} - \phi_r\nabla \cdot \mathbf{n} \\ &= (\phi_{rr}\mathbf{n} + \phi_r\mathbf{n}_r) \cdot \mathbf{n} - \phi_r\nabla \cdot \mathbf{n} = \phi_{rr} + (\kappa_1 + \kappa_2)\phi_r. \end{aligned}$$

where κ_1 and κ_2 are the principal curvatures of the surface. Since the divergence of unit normal vector to a surface is equal to the negative of mean curvature ($\kappa_1 + \kappa_2$), the last equality holds. Then, we can have it for the kinetic equation:

$$\phi_t = -\frac{F'(\phi)}{\epsilon^2} + \phi_{rr} + (\kappa_1 + \kappa_2)\phi_r, \tag{2.1}$$

For the planar interface at equilibrium, the following equation holds

$$-\frac{F'(\phi)}{\epsilon^2} + \phi_{rr} \approx 0. \tag{2.2}$$

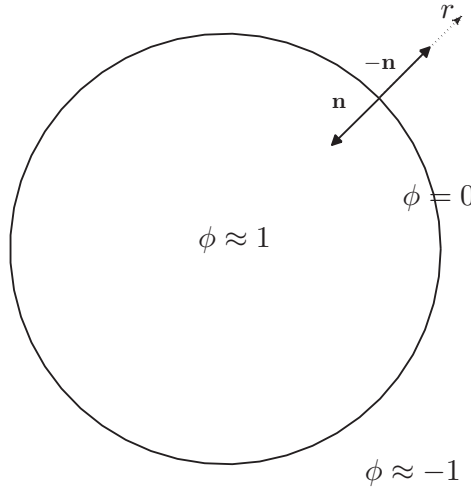


FIGURE 1. Illustration of an interface showing the order parameter, ϕ , and unit normal, \mathbf{n} .

Therefore, equation (2.1) can be rewritten as

$$\phi_t = (\kappa_1 + \kappa_2)\phi_r. \tag{2.3}$$

At all times, we denote the zero level-set by $\Gamma_t = \{(x, y, z) | \phi(x, y, z, t) = 0\}$. Then, the velocity of zero level-set Γ_t is given by

$$0 = \left. \frac{d(\phi(r, t))}{dt} \right|_{\Gamma_t} = \phi_r r_t + \phi_t \Rightarrow r_t = -\phi_t / \phi_r = -(\kappa_1 + \kappa_2). \tag{2.4}$$

Therefore, all surfaces between two phases move with the velocity V , which is given by

$$V = -(\kappa_1 + \kappa_2) = -\left(\frac{1}{R_1} + \frac{1}{R_2}\right), \tag{2.5}$$

where R_1, R_2 are the principal radii of curvatures at the point of the surface.

3 Numerical scheme

In this section, for simplicity of exposition, we describe a numerical scheme for the AC equation in two dimensions. A three-dimensional numerical scheme is analogously defined. A computational domain is partitioned into a uniform mesh with mesh size h . The centre of each cell, Ω_{ij} , is located at $\mathbf{x}_{ij} = (x_i, y_j) = (a + (i - 0.5)h, b + (j - 0.5)h)$ for $i = 1, \dots, N_x$ and $j = 1, \dots, N_y$. Here, N_x and N_y are the numbers of cells in the x - and y -directions, respectively. Let ϕ_{ij}^n be approximations of $\phi(x_i, y_j, n\Delta t)$, where $\Delta t = T/N_t$, T , and N_t are the temporal step size, final time, and the total number of time steps, respectively.

We use the unconditionally stable hybrid numerical method for solving the AC equation [56]. The method is based on an operator splitting method [65], which is to split the original

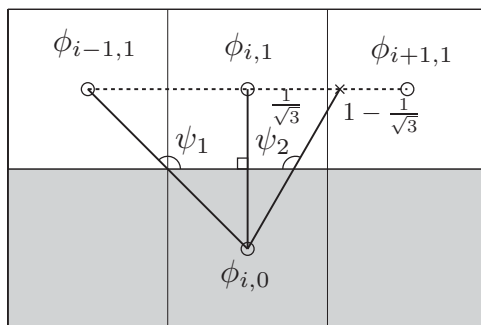


FIGURE 2. The point $\phi_{i,0}$ is defined in an exterior domain Ω for contact angle boundary conditions.

problem into a sequence of simpler problems:

$$\phi_t = \Delta\phi, \tag{3.1a}$$

$$\phi_t = \frac{\phi - \phi^3}{\epsilon^2}. \tag{3.1b}$$

As a first step, we solve equation (3.1a) by applying the Crank–Nicolson method, that is,

$$\frac{\phi_{ij}^* - \phi_{ij}^n}{\Delta t} = \frac{1}{2}(\Delta_h \phi_{ij}^* + \Delta_h \phi_{ij}^n), \tag{3.2}$$

where Δ_h is the standard five point discretization. As a next step, equation (3.1b) is solved analytically and the solution is given by

$$\phi_{ij}^{n+1} = \frac{\phi_{ij}^*}{\sqrt{e^{-\frac{2\Delta t}{\epsilon^2}} + (\phi_{ij}^*)^2 \left(1 - e^{-\frac{2\Delta t}{\epsilon^2}}\right)}}. \tag{3.3}$$

For more details of the unconditionally stable hybrid scheme, we refer the reader to [56].

For the contact angle boundary condition considered here, we implement the interpolation scheme introduced in [55] for the Cahn–Hilliard equation. Figure 2 illustrates the interpolation stencil for contact angles. When we have contact angle $\psi_1 = 3\pi/4$ on boundary, boundary values are given by

$$\phi_{i,0}^{n+1} = \begin{cases} \phi_{i+1,1}^{n+1} & \text{if } \phi_{i-1,1}^{n+1} > \phi_{i+1,1}^{n+1}, \\ \phi_{i-1,1}^{n+1} & \text{otherwise.} \end{cases}$$

Similarly, we can extend this scheme to various contact angles by interpolations. For instance, if the prescribed angle $\psi_2 = -5\pi/6$ is given, then the boundary treatment is as follows:

$$\phi_{i,0}^{n+1} = \begin{cases} \left(1 - \frac{1}{\sqrt{3}}\right) \phi_{i,1}^{n+1} + \frac{1}{\sqrt{3}} \phi_{i+1,1}^{n+1} & \text{if } \phi_{i-1,1}^{n+1} < \phi_{i+1,1}^{n+1}, \\ \frac{1}{\sqrt{3}} \phi_{i,1}^{n+1} + \left(1 - \frac{1}{\sqrt{3}}\right) \phi_{i+1,1}^{n+1} & \text{otherwise.} \end{cases}$$

Table 1. l_2 -norm of the errors and convergence rates.

x-axis grid	64–128	Rate	128–256	Rate	256–512
l_2	36.276e-4	2.02	8.9240e-4	1.97	2.2721e-4

To obtain an estimate of the rate of convergence, we perform a number of simulations on increasingly finer grids. The initial data is given by

$$\phi(x, y, 0) = \tanh \frac{0.3 - \sqrt{(x - 0.5)^2 + (y - 0.3/\sqrt{2})^2}}{\sqrt{2}\epsilon}$$

on the computational domain, $\Omega = (0, 1) \times (0, 1)$ with $\epsilon = 0.01$, contact angles $\psi_1 = \pi/4$, $\psi_2 = -\pi/4$, and temporal step size $\Delta t = 1.0 \times 10^{-5}h$. The numerical solutions are computed on the uniform grids $\Delta x = \Delta y = 1/2^n = h$ for $n = 6$ to 9. For each simulation, the calculation is run to time $T = 2.5 \times 10^{-5}$. We define the error of a grid to be the discrete l_2 -norm of the difference between that grid and the average of the next finer cells covering it:

$$e_{h/\frac{1}{2}ij} := \phi_{hij} - (\phi_{\frac{1}{2}2i,2j} + \phi_{\frac{1}{2}2i-1,2j} + \phi_{\frac{1}{2}2i,2j-1} + \phi_{\frac{1}{2}2i-1,2j-1})/4.$$

Also, the rate of convergence is defined by $\log_2(\|e_{h/\frac{1}{2}}\|/\|e_{h/4}\|)$ and this is the ratio of successive errors. Table 1 shows the errors and rates of convergence. These results suggest that it is the second-order scheme [55].

4 Numerical experiments for the mean curvature flow without the boundary conditions

In this section, we present numerical experiments including basic mechanism for interface evolutions by the AC equation, then the numerical scheme of the equation is employed for the curvature driven flow for a convex and enclosed curve and three-dimensional surface.

The interfacial width $\epsilon_m > 0$, where $m > 0$, is used for a measure of the thickness across the diffuse-interface. If we consider that the order parameter ϕ varies from -0.9 to 0.9 over the interfacial region with m grid points, the ϵ value is defined by $\epsilon = \epsilon_m = hm/(2\sqrt{2}\tanh^{-1}(0.9))$ [56]. Here h is the uniform mesh size.

4.1 Basic mechanism for interface evolutions

Figures 3(a) and (b) show the numerical evolutions when the initial curve of the zero level-set has positive constant mean curvature (circle) and zero mean curvature (straight line), respectively. The first columns in Figures 3(a) and (b) show the initial profiles ϕ^0 for the circle and the straight line. Using the initial data, we get the intermediate solution, ϕ^* , by solving equation (3.1a) and it is shown in the second column. Next, we solve equation (3.1b) to get ϕ^1 which is shown in the third column. In the circle case, Figure 3(a), the diffusion step smoothes interfacial region, resulting in shrinking the zero level curve of the phase-field, (see the second column in Figure 3(a)). Next, the sharpening step makes

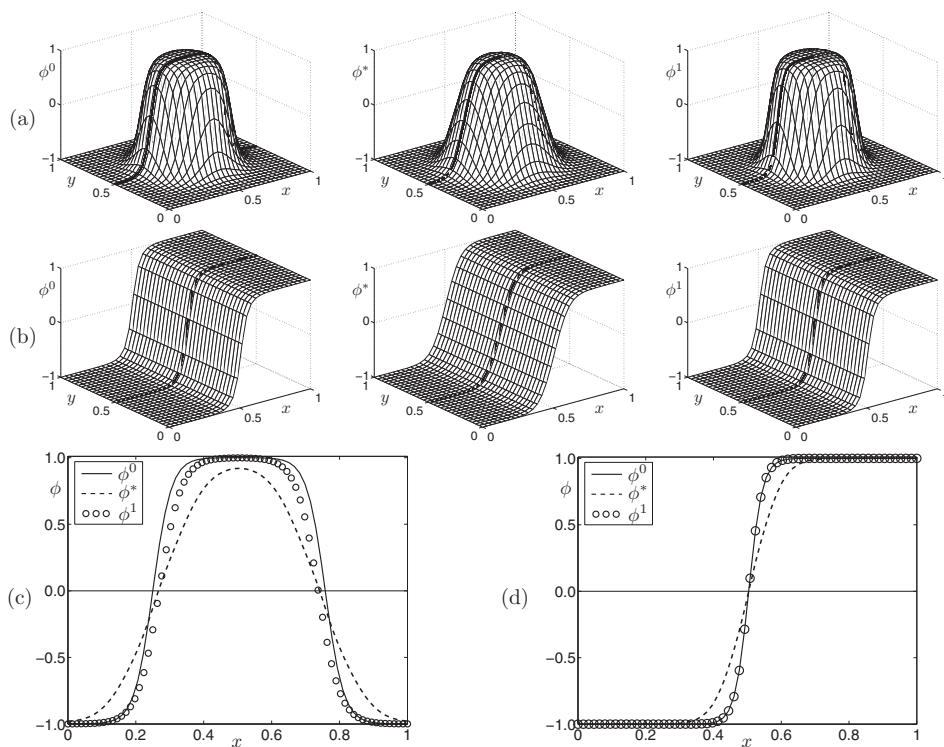


FIGURE 3. (a) and (b) are the one time step evolutions of ϕ whose initial zero level-sets represent a circle and a straight line, respectively. (c) and (d) are cross sectional profiles of (a) and (b) at $y = 0.5$, respectively.

the phase-field approach ± 1 depending on its sign while keeping the zero level-set fixed (the third column in Figure 3(a)). Continuing this process, the zero level curve shrinks to a point. In the straight line case, Figure 3(b), neither the diffusion step nor the sharpening step affects the zero level curve. Figures 3(c) and (d) are the cross-sectional plots of ϕ^0 , ϕ^* , and ϕ^1 at $y = 0.5$ in Figures 3(a) and (b), respectively.

4.2 Curve-shortening flow for a convex and closed curve

A curve is called a convex curve if it is a curve with positive curvature. We show that the curve-shortening flow evolves a convex and closed curve into a round circle and the area enclosed by a curve decreases with a fixed rate, and consequently a curve shrinks to a point and disappears in finite time. We first introduce the idea of defining a convex curve in terms of its support function.

Definition 4.1 Let γ be a convex and planar curve and $O \in \mathbb{R}^2$ the origin. The function $S(p)$ is assigned to each point $p \in \gamma$ for the distance between O and the straight line tangent to γ at p . In differential geometry, the function S is called the support function [45].

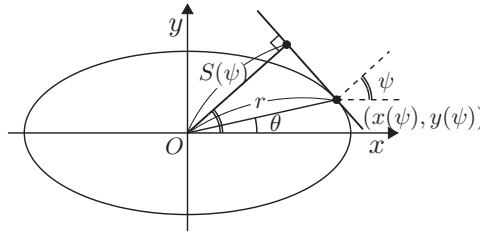


FIGURE 4. Definitions for the support function.

Since the support function S is the tangent line to γ at p , a convex curve may be given as a function of the angle ψ between S and the x -axis. We note that $p = (x(\psi), y(\psi))$, and the point p is given in polar coordinates as $re^{i\theta}$. A convex curve may be given as a function of the angle $\psi = \theta - \pi/2$ of the normal with x -axis, where θ is the tangent angle. If there is a tangent line passing a point $(x(\psi), y(\psi))$ where the normal is given by $-(\cos \psi, \sin \psi)$, the support function S is the signed distance from the origin to the line. Thus, the function measures the distance from the tangent line at $(x(\psi), y(\psi))$ to the origin O . Let us also follow the notations in Figure 4. For a convex curve, it is convenient to use the support function. With the help of the support function, we can show the following lemma. It also appears in [76].

Lemma 1 (Zhu [76]) *The curvature satisfies that*

$$\kappa = \frac{1}{S_{\psi\psi} + S}.$$

Proof Let us denote the support function of the curve by S . We write (r, θ) for polar coordinates, and $\gamma(\psi) := (x(\psi), y(\psi))$ for corresponding Cartesian coordinates at a point on a curve. Here ψ is the angle between x -axis and the perpendicular line to the tangent line at the point as shown in Figure 4. Then, the support function $S(\psi)$ is given by:

$$\begin{aligned} S(\psi) &= r \cos(\psi - \theta) = r(\cos \theta \cos \psi + \sin \theta \sin \psi) = x(\psi) \cos \psi + y(\psi) \sin \psi \\ &= \gamma(\psi) \cdot (\cos \psi, \sin \psi) = -\gamma(\psi) \cdot \mathbf{n}. \end{aligned}$$

Its derivative satisfies $S_{\psi}(\psi) = -x(\psi) \sin \psi + y(\psi) \cos \psi$. By direct computation, the curve can be represented by the support function

$$\begin{aligned} x(\psi) &= S(\psi) \cos \psi - S_{\psi}(\psi) \sin \psi, \\ y(\psi) &= S(\psi) \sin \psi + S_{\psi}(\psi) \cos \psi. \end{aligned} \tag{4.1}$$

In fact, the curvature can be written as [40]

$$\kappa = \frac{\dot{x}\dot{y} - \ddot{x}\dot{y}}{(\dot{x}^2 + \dot{y}^2)^{3/2}} = \frac{1}{S_{\psi\psi} + S}. \tag{4.2}$$

To see this, we use the parameter $p \in I$, where $I = [0 + \psi_1, 2\pi + \psi_2]$, where $0 \leq \psi_1 \leq \pi$ and $-\pi \leq \psi_2 \leq 0$. Here, we assume that $\gamma(p, t) : I \times [0, \omega) \rightarrow \mathbb{R}^2$ is a family of convex

curves satisfying the curve-shortening flow $\gamma_t = \kappa \mathbf{n}$. Let us use the normal angle θ of the support function to parameterize convex curves, and we change variable forms (p, t) to (θ, τ) . Consequently, the time derivative of the support function can be written as

$$\frac{\partial S}{\partial \tau} = \left(\frac{\partial \gamma}{\partial p} \frac{\partial p}{\partial \tau} + \kappa \mathbf{n}, -\mathbf{n} \right) = -\kappa = \frac{-1}{S_{\psi\psi} + S}.$$

Note that $\partial/\partial t$ is the partial derivative with fixed p while $\partial/\partial \tau$ is the partial derivative with fixed θ , i.e., $\partial/\partial t \neq \partial/\partial \tau$ [40]. □

Theorem 4.2 (Gage and Hamilton [40]) *The area $A(t)$ enclosed by the curve decreases at constant rate*

$$\frac{dA(t)}{dt} = -2\pi,$$

provided that it follows the curve-shortening flow equation.

Proof It is well known that the area decreases at constant rate [40, 76]. Let us suppose that the area $A(t)$ is enclosed by the curve at time t . Then, area formula is given by Green’s theorem

$$\begin{aligned} A(t) &= \frac{1}{2} \int_0^{2\pi} (x\dot{y} - y\dot{x}) d\psi = \frac{1}{2} \int_0^{2\pi} (x \cos \psi + y \sin \psi)(-\dot{x} \sin \psi + \dot{y} \cos \psi) d\psi \\ &= \frac{1}{2} \int_0^{2\pi} S(S_{\psi\psi} + S) d\psi = \frac{1}{2} \int_0^{2\pi} \frac{S}{\kappa} d\psi. \end{aligned} \tag{4.3}$$

By taking derivative of equations (4.2) and (4.3) with respect to time, and integrating by parts, we have

$$\begin{aligned} \frac{dA(t)}{dt} &= \frac{1}{2} \int_0^{2\pi} \frac{\partial}{\partial t} \left(\frac{S}{\kappa} \right) d\psi = \frac{1}{2} \int_0^{2\pi} \left(\frac{S_t}{\kappa} - \frac{S\kappa_t}{\kappa^2} \right) d\psi \\ &= -\frac{1}{2} \int_0^{2\pi} [1 + (S_{\psi\psi} + S)\kappa] d\psi = -2\pi. \end{aligned}$$

Thus, we find the area function for time t : $A(t) = A(0) - 2\pi t$. We remark that any embedded closed curve has the same property:

$$\frac{d}{dt} A(t) = - \int_{\gamma_t} \kappa ds = - \int_0^{2\pi} d\theta = -2\pi. \tag{4.4}$$

□

Equation (4.3) demonstrates that $A(t)$ enclosed by a convex-closed curve decreases at a constant rate -2π , and the maximal time ω is given by $\omega = A(0)/(2\pi)$. To see that, we set two different initial curves having the same area as $A(0) = 0.16\pi$. The initial curves are represented by

$$\phi(x, y, 0) = \tanh \frac{1 - \sqrt{(x/a)^2 + (y/b)^2}}{\sqrt{2}\epsilon_6}, \tag{4.5}$$

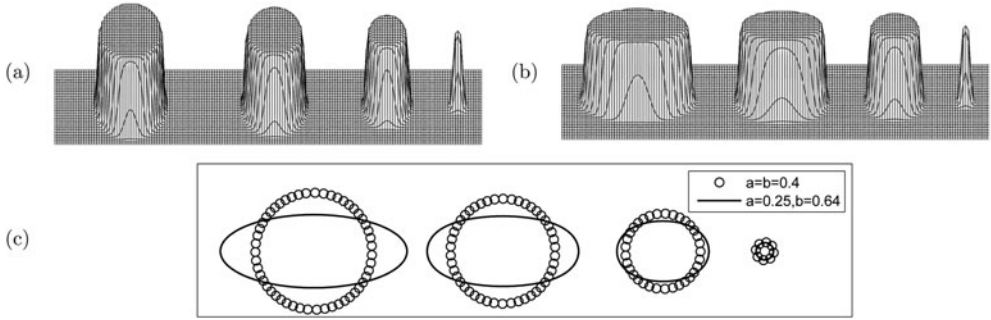


FIGURE 5. (a) Evolution of a circle, (b) evolution of an ellipse and (c) comparison of two evolutions.

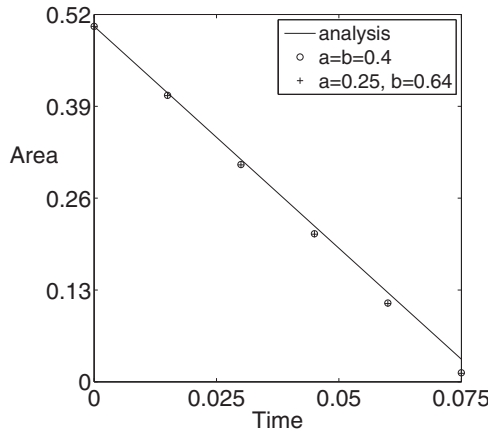


FIGURE 6. The areas of circle and ellipse decrease as time passes.

for the case of circle: $a = b = 0.4$ and the case of ellipse: $a = 0.25, b = 0.64$. A 256×256 grid is used on the domain $\Omega = (-0.8, 0.8) \times (-0.8, 0.8)$. We choose $h = 1.6/256$, $\Delta t = 2.5 \times 10^{-5}$ and the computations run until the final time $T = 0.075$. Figures 5(a)–(c) show the evolution of circle and ellipse. From left to right, curve profiles are plotted in temporal order, $t = 0, t = 0.0156, t = 0.0468$, and $t = 0.078$, respectively. In the lower plot (c), the zero level curve is shown to represent the shrinking curve. Figure 6 shows the numerical results and theoretical predictions of the decreasing rate of the area.

4.3 Enclosed surface

Theorem 4.3 (Huisken [49]) *et γ_1 and γ_2 the two convex curves evolve according to the curvature flow in the plane, and γ_1 contains the closed curve γ_2 , then the curve is enclosed by γ_1 for all $t \in [0, \omega)$.*

Proof It is called the containment principle [76]. One can prove this by applying the comparison principle for parabolic partial differential equations [54]. We let $S_1(\psi, t)$ and $S_2(\psi, t)$ be the support functions of γ_1 and γ_2 , respectively. Then, the containment

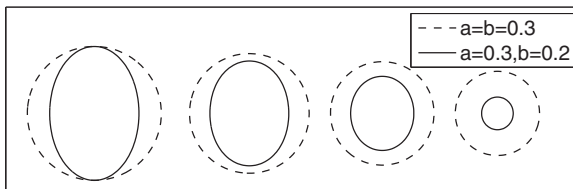


FIGURE 7. From left to right, two curves are contour of zero level-set at the following time $t = 0$, $t = 0.009$, $t = 0.018$, and $t = 0.027$.

argument, so called, is satisfied by applying the maximum principle of parabolic equations. One deduces that $S_2(\theta, t) \leq S_1(\theta, t)$ for all $t \in [0, \omega)$ [29, 58, 76]. \square

For example, suppose that the inner circle is enclosed by the outer ellipse at initial time $t = 0$. Then, the inner circle is bounded by the outer circle for all $t \in (0, \omega)$. In addition to that, the containment principle holds for the three-dimensional case if one convex-closed surface Γ_1 is enclosed by the other convex-closed surface Γ_2 . In fact, these follow from the work by Huisken [49].

To observe that, we perform the test on two-dimensional domain $\Omega = (0, 1) \times (0, 1)$ with mesh size $h = 1/256$, and take the initial condition as

$$\phi(x, y, 0) = \tanh \frac{1 - \sqrt{((x - 0.5)/a)^2 + ((y - 0.5)/b)^2}}{\sqrt{2}\epsilon_6}. \tag{4.6}$$

Here, the parameters $a = b = 0.3$ and $a = 0.3, b = 0.2$ are used for one circle enclosing the other ellipse. The computations run until final time $T = 0.027$ with the temporal step size $\Delta t = 10^{-5}$. Figure 7 shows the oval curve is always enclosed by a circle. Thus, the containment principle is satisfied.

Theorem 4.4 (avoidance principle [29, 76]) *Any two smooth solutions of the mean curvature flow which are disjoint, then they stay disjoint.*

By applying the standard comparison principle, we can obtain the same result in higher dimensions, (see [29] and references therein). For a three-dimensional test we describe the following sphere which encloses the ellipsoid, (see Figure 8). The computational domain is $\Omega = (0, 2) \times (0, 2) \times (0, 2)$ with a $128 \times 128 \times 128$ mesh grid and the initial configuration is given by

$$\phi(x, y, z, 0) = \tanh \frac{1 - \sqrt{((x - 1)/a)^2 + ((y - 1)/b)^2 + ((z - 1)/c)^2}}{\sqrt{2}\epsilon_6}.$$

Here $a = b = c = 0.8$ and $a = 0.8, b = c = 0.6$ are used for the sphere and ellipsoid, respectively. Figures 8(a) and (b) show the zero level-set of the sphere and ellipsoid at the initial time. Simulations evolved in time are put together to form as shown in Figures 8(c)–(e). This example shows that the mean curvature flow in higher dimensions evolves convex surfaces into a point, and keeps them disjoint.

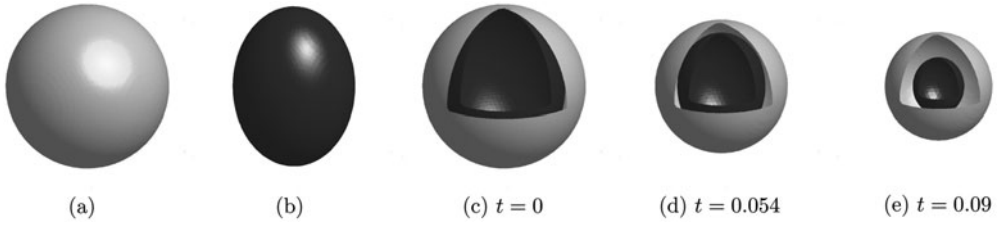


FIGURE 8. (a) and (b): the zero level isosurfaces of sphere and ellipsoid at initial time. (c)–(e): two evolutions are plotted together in temporal order.

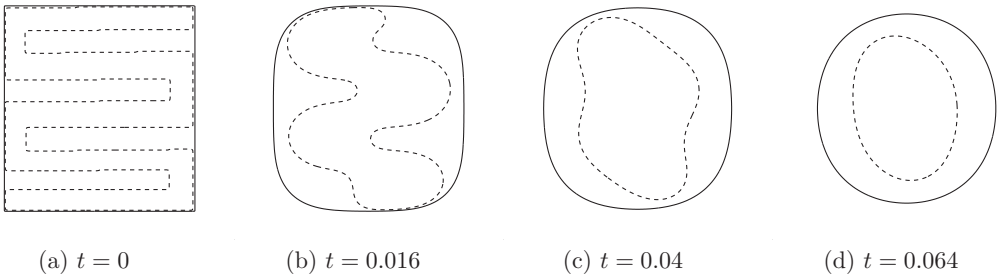


FIGURE 9. Temporal evolution of a non-convex initial curve. (a) $t = 0$, (b) $t = 0.016$, (c) $t = 0.04$, (d) $t = 0.064$.

4.4 Non-convex curve-shortening flow

Theorem 4.5 (Grayson’s convexity theorem) *A non-convex embedded curve converges to a round circle.*

It is guaranteed by Grayson [42] that any closed and smooth planar curve converges to a round circle under the curve-shortening flow. Furthermore, there exists a time t_0 such that the curve is convex for all $t \in [t_0, \omega)$. To verify Grayson’s theorem, we perform a numerical experiment with a non-convex initial curve as shown in Figure 9(a). Numerical solutions are obtained on $\Omega = (0, 1) \times (0, 1)$ using a 256×256 mesh grid. $\epsilon = \epsilon_6$ and $\Delta t = 10^{-5}$ are used.

It is also important to note that Grayson’s convexity theorem only holds for the curve-shortening flow in planar case. In general, it is not satisfied for the mean curvature flow in more than two-dimensional space. A simple example is a dumbbell-shaped surface in the three-dimensional space [56].

4.5 Three dimensional cylinder

Theorem 4.6 (Huisken [49]) *If a strictly convex surface is evolved by the mean curvature flow, then it stays convex until it shrinks to a point.*

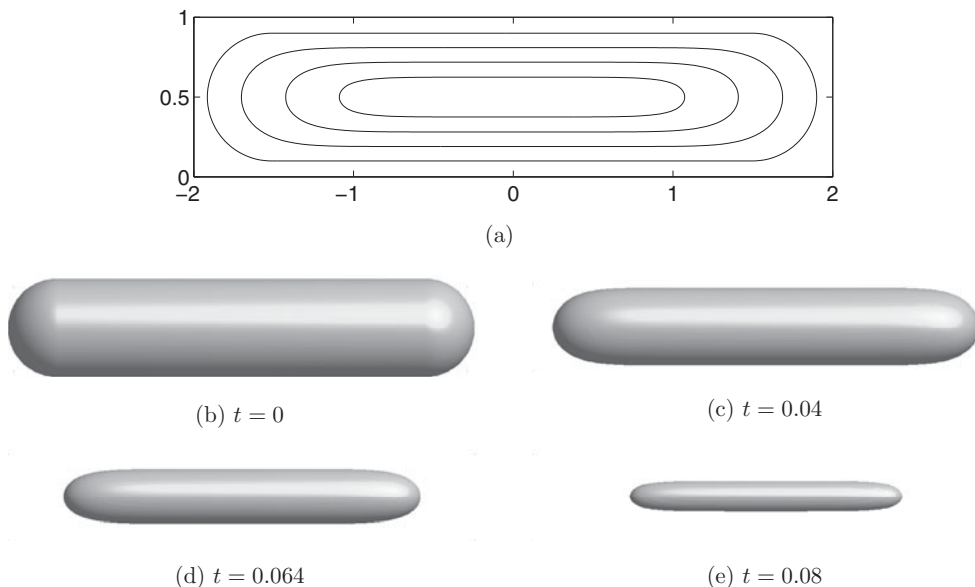


FIGURE 10. Motion of a capped off cylinder.

Now we consider the thin cylinder for initial data, which is capped off at two ends, (see Figure 10(b)). The initial configuration is defined as follows:

$$\phi(x, y, z, 0) = \begin{cases} \tanh \frac{0.4 - \sqrt{x^2 + (y-0.5)^2 + (z-0.5)^2}}{\sqrt{2}\epsilon_6} & \text{if } |x| < 1.5 \\ \tanh \frac{0.4 - \sqrt{(x-0.5)^2 + (y-0.5)^2 + (z-0.5)^2}}{\sqrt{2}\epsilon_6} & \text{if } x \geq 1.5 \\ \tanh \frac{0.4 - \sqrt{(x+1.5)^2 + (y-0.5)^2 + (z-0.5)^2}}{\sqrt{2}\epsilon_6} & \text{if } x \leq -1.5 \end{cases}$$

In the simulation, a $128 \times 64 \times 64$ mesh is used on $\Omega = (-2, 2) \times (0, 1) \times (0, 1)$ and we employ $\Delta t = 2.0 \times 10^{-5}$, $T = 0.09$ and ϵ_6 . Unlike an example of the dumbbell shape in the three-dimensional space [43], the surface neither pinches off nor splits into two surfaces as shown in Figures 10(b)–(e).

5 Numerical experiments for the curve-shortening flow with prescribed contact angles

Let γ be a smooth curve with prescribed contact angles ψ_1 and ψ_2 . If κ is the curvature and \mathbf{n} is the outward unit normal, then we call that γ evolves by the curve-shortening flow with prescribed angles ψ_1 and ψ_2 if

$$\frac{\partial \gamma}{\partial t}(s, t) = \kappa(s, t)\mathbf{n}(s, t) \quad (s, t) \in [0, 1] \times [0, \omega) \quad \text{for some } 0 < t < \omega,$$

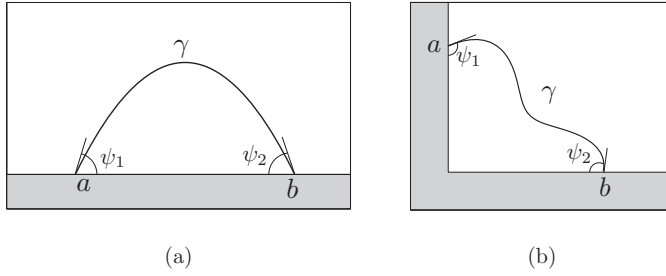


FIGURE 11. (a) boundary of the upper half-plane, and (b) boundary of the first quadrant.

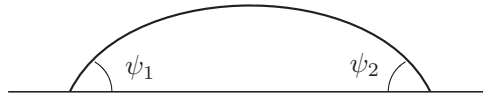


FIGURE 12. The initial curve with the prescribed contact angles ψ_1 and ψ_2 .

where $\psi_1 \in (0, \pi)$ and $\psi_2 \in (-\pi, 0)$. Let us first consider the parameterized curve $\gamma_t := \mathbf{X}(s, t) = (x(s, t), y(s, t))$, then we have

$$\mathbf{T} = \frac{\mathbf{X}_s}{|\mathbf{X}_s|} = \frac{(x_s, y_s)}{\sqrt{x_s^2 + y_s^2}}, \quad \mathbf{n} = \frac{(y_s, -x_s)}{\sqrt{x_s^2 + y_s^2}},$$

$$\mathbf{V} = (x_t, y_t) \cdot \mathbf{n}, \quad \text{and} \quad \kappa = \frac{\mathbf{X}_{ss}}{|\mathbf{X}_s|^2} \cdot \mathbf{n}.$$

If we consider a solution of the curve-shortening flow where the curve γ is represented by the graph form $y = u(x)$, $x \in [a, b]$ where a and b are end points, we have the geometrical quantities at $(x, u(x, t))$:

$$\mathbf{T} = \frac{(1, u_x)}{\sqrt{1 + u_x^2}}, \quad \mathbf{n} = \frac{(u_x, -1)}{\sqrt{1 + u_x^2}},$$

$$\mathbf{V} = \frac{-u_t}{\sqrt{1 + u_x^2}}, \quad \text{and} \quad \kappa = \frac{-u_{xx}}{(1 + u_x^2)^{\frac{3}{2}}} = \frac{(\arctan u_x)_x}{\sqrt{1 + u_x^2}}.$$

Let a curve γ_t on interval $[a, b]$ be a smooth solution of the curvature flow, and intersect with prescribed angles ψ_1 and ψ_2 , on the boundary. Thus, we have the following equations

$$u_t = (\arctan(u_x))_x, \quad x \in (a(t), b(t)), \quad t \in (0, \omega),$$

$$u(a, t) = 0, \quad u(b, t) = 0,$$

$$u_x(a, t) = \tan \psi_1, \quad u_x(b, t) = \tan \psi_2.$$

We begin the numerical experiments with an arc of a circle and radius $r = 1$. It meets a boundary with the prescribed contact angles $\psi_1 = \pi/4$ and $\psi_2 = -\pi/4$, (see Figure 12). Here, we consider the effect of $\epsilon = \epsilon_m$, where $m = 4, 6, 8$, and 16 in equation (3.3). The

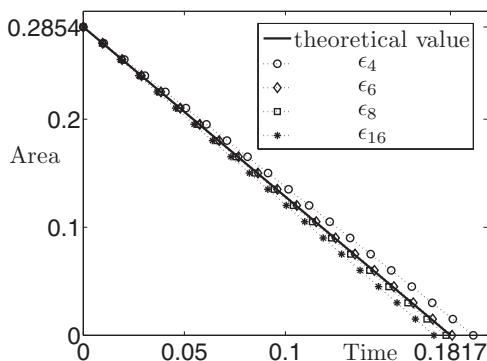


FIGURE 13. The area of an arc decreases with different values of ϵ_m .

initial data is given by

$$\phi(x, y, 0) = \tanh \frac{1 - \sqrt{x^2 + (y - 2/\sqrt{2})^2}}{\sqrt{2}\epsilon_m}.$$

on the domain $\Omega = (-1, 1) \times (0, 1)$. The numerical solutions are computed on the uniform grid $h = 1/256$, temporal step size $\Delta t = 5 \times 10^{-6}$ and various ϵ_m . For each ϵ_m where $m = 4, 6, 8$ and 16 , the calculation is run to time until it vanishes at $T_4 = 0.1930$, $T_6 = 0.1825$, $T_8 = 0.1795$ and $T_{16} = 0.1735$ as shown in Figure 13. The area of a segment of a circle is equal to $\pi/4 - 1/2$ and it vanishes at $\omega = 0.1817$ under the curve-shortening flow. Note that the solution of the AC equation theoretically follows motion by mean curvature as ϵ goes to zero. However, there is a numerical restriction on spatial step size. Therefore, it is also important to set the value of ϵ_m comparing with spatial step sizes. In the simulations, there is a good match in the ϵ_6 and ϵ_8 .

5.1 Losing a graph property

For a smooth curve, we should prescribe contact angles $0 < \psi_1 < \pi$, $-\pi < \psi_2 < 0$ and $|\psi_1| + |\psi_2| = \pi$ with a graphical solution to avoid the blow-up of the graph [22]. We show an example where a curve evolved by the curvature flow loses the graph property with the contact angle boundary conditions. Assume that we have the parameterized curve $\gamma(t)$ with the same conditions (5.3), but it violates the condition of preserving a graph property. Then, the curve may pinch off along the boundary, and become singular. Figure 14 shows the evolution of an arc with prescribed contact angles $\psi_1 = 154.4^\circ$ and $\psi_2 = -154.4^\circ$. The boundary angle conditions are given by

$$\phi_{i,0}^{n+1} = \begin{cases} \phi_{i-2,1}^{n+1} & \text{if } \phi_{i-1,1}^{n+1} < \phi_{i+1,1}^{n+1}, \\ \phi_{i+2,1}^{n+1} & \text{otherwise.} \end{cases}$$

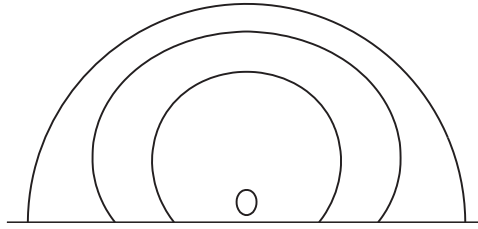


FIGURE 14. Evolution of the curve with prescribed angles $\psi_1 = 154.4^\circ$ and $\psi_2 = -154.4^\circ$.

We put the upper semi-circle, where the centre of the unit circle is at $(1.5, 0)$, as the initial condition on domain $\Omega = (0, 3) \times (0, 1.5)$. The initial configuration is given by

$$\phi_{ij}^0 = \tanh(1 - \sqrt{(x - 1.5)^2 + y^2}) / \sqrt{2}\epsilon_6.$$

The simulation parameters are given by $\epsilon_6, h = 3/256, \Delta t = 6.34 \times 10^{-6}$, and mesh size 256×128 . Figure 14 shows the evolutions of the curve. In this case, pinching off along the axis is observed.

5.2 Preserving convexity

Theorem 5.1 *A convex curve with contact angles $0 < \psi_1 < \pi/2$ and $-\pi/2 < \psi_2 < 0$ preserves convexity.*

Proof As before, we use the support function (4.2) on ψ . By taking derivative in time, the support function can be written as

$$\frac{\partial S}{\partial t} = \frac{d\gamma}{dt} \cdot (\cos \psi, \sin \psi) = \kappa \mathbf{n} \cdot (\cos \psi, \sin \psi) = -\kappa = \frac{-1}{S_{\psi\psi} + S}.$$

The derivative of the curvature κ with respect to time is

$$\begin{aligned} \frac{d\kappa}{dt} &= \left(\frac{1}{S_{\psi\psi} + S} \right)_t = -\frac{1}{(S_{\psi\psi} + S)^2} (S_{\psi\psi t} + S_t) = -\kappa^2 [(-\kappa)_{\psi\psi} - \kappa] \\ &= \kappa^2 (\kappa_{\psi\psi} + \kappa). \end{aligned}$$

By a direct application of the maximum principle, we obtain

$$\min_{\psi \in I} \kappa(\psi, t) \geq \min_{\psi \in I} \kappa(\psi, 0) > 0, \quad t \in [0, \omega]. \tag{5.1}$$

Now let us assume the curvature κ is bounded below in $I := (a(0), b(0))$ by $\lambda > 0$ for a convex curve. Set $\lambda > \sup \kappa^2$ on $I \times [0, \omega]$ and suppose $\kappa < 0$ at some point on I . If we define $w = e^{-\lambda t} \kappa$, then minimum of w is negative. Let $(\bar{\psi}, \bar{t})$ be the minimum point of w on I . The time derivative of w is as follows

$$w_t = -\lambda e^{-\lambda t} \kappa + e^{-\lambda t} \kappa_t = -\lambda e^{-\lambda t} \kappa + e^{-\lambda t} (\kappa_{\psi\psi} + \kappa) \kappa^2. \tag{5.2}$$

Since we have the minimum at $(\bar{\psi}, \bar{t})$, the following inequalities hold:

$$w_t(\bar{\psi}, \bar{t}) \leq 0, \quad w(\bar{\psi}, \bar{t}) < 0 \quad \text{and} \quad w_{\psi\psi} \geq 0.$$

This means that the equality (5.2) can be written as

$$\begin{aligned} w_t &= -\lambda e^{-\lambda t} e^{\lambda t} w + e^{-\lambda t} (e^{\lambda t} w_{\psi\psi} + e^{\lambda t} w) \kappa^2 = -\lambda w + w_{\psi\psi} + w \kappa^2 \\ &= w(\kappa^2 - \lambda) + w_{\psi\psi} > 0. \end{aligned}$$

But this contradicts the assumption. □

5.3 Convergence to a point

Theorem 5.2 *If there is a curve intersecting with prescribed contact angles, then shrinking to an arc of the round circle by the curve-shortening flow needs the following condition:*

$$\cos \psi_1 + \cos \psi_2 = 0.$$

Proof The area decreases to zero, then it must be a point or a line segment. If the curvature flow develops a line segment, it is clear that minimum of the curvature is zero. But we have positive lower bound on κ from (5.1), the curve shrinks to a point when prescribed angles ψ_1 and ψ_2 belong to $(0, \pi/2)$ and $(-\pi/2, 0)$, respectively.

We consider that the curve segment may not develop a round circle, and then give a necessary condition which is required as a contact-angle boundary condition for a curve γ_t converging to the round circle at t . Let $p, q \in \gamma_t$ be two points in curve γ_t at t . We first define intrinsic distance l_t and extrinsic distance d_t as follows $d_t, l_t : \gamma_t \times \gamma_t \times [0, \omega] \rightarrow \mathbb{R}$

$$l_t(p, q, t) = \int_p^q ds_t, \quad d_t(p, q, t) = |\gamma_t(p, t) - \gamma_t(q, t)|.$$

Suppose that the curve γ_t converges to the segment of circle with perimeter L_t at t . We define the function by

$$\Phi_t(p, q) = \frac{\pi d_t}{L_t} / \sin \frac{\pi l_t}{L_t}.$$

In addition, we define the embeddedness ratio

$$E(t) := \min_{p, q} \Phi_t(p, q).$$

Since we assume that the curve γ_t converges to the part of round circle, we have the ratio $E(t) \equiv 1$ at t [50].

Next, we set $p(s)$ with $p = a$ and $q = b$ and $\alpha := \pi l_t / L_t$, by the assumption we have

$$0 = \frac{d}{ds} \Phi_t(p(s), q) \Big|_{s=0} = \frac{\pi}{L_t} \frac{\langle p - q, \tau(p) \rangle}{d_t \sin \frac{\pi l_t(p, q)}{L_t}} - \frac{\pi d_t}{L_t \sin^2 \frac{\pi l_t(p, q)}{L_t}} \frac{\pi \cos \frac{\pi l_t(p, q)}{L_t}}{L_t},$$

where we denote the oriented unit tangent vector to γ_t at p by $\tau(p)$. By this, we get

$$\cos \beta(p) = \frac{\langle p - q, \tau(p) \rangle}{d_t} = \frac{\pi d_t}{L_t \sin \frac{\pi l_t(p,q)}{L_t}} \cos \frac{\pi l_t(p,q)}{L_t} = E(t) \cos \alpha.$$

Here $\beta(p)$ is the angle between the vectors $p - q$ and $\tau(p)$. Similarly, we can get the following equation for the point q

$$\cos \beta(q) = -E(t) \cos \alpha.$$

Since we assume that $E \equiv 1$,

$$\cos \beta(p) + \cos \beta(q) = 0,$$

where $\beta(a) = \psi_1$ and $\beta(b) = \psi_2$. □

5.4 Decreasing area

Consider a solution of the curvature flow where the parameterized curve $\gamma : [0, 1] \times \mathbb{R} \rightarrow \mathbb{R}^2$ is of the graph $\phi(x, t) : \mathbb{R} \times \mathbb{R} \rightarrow \mathbb{R}_+$ with fixed endpoint conditions

$$\begin{aligned} \gamma(0, t) &= (a(t), 0), & \gamma(1, t) &= (b(t), 0), \\ \phi(a(t), t)_x &= \tan \psi_1, & \phi(b(t), t)_x &= \tan \psi_2, \quad 0 < \psi_1 < \frac{\pi}{2} \quad \text{and} \quad -\frac{\pi}{2} < \psi_2 < 0, \end{aligned} \tag{5.3}$$

where \mathbb{R}_+ is the set of non-negative real numbers, and we note that two points $(a(t), 0), (b(t), 0) \in \mathbb{R}^2$, $a(t) < b(t)$ are end points along x -axis. For one dimension, the equation of the curvature flow is written in the form:

$$\frac{\partial u}{\partial t} = \frac{u_{xx}}{(1 + u_x^2)} = (\arctan u_x)_x. \tag{5.4}$$

Theorem 5.3 *Assume that prescribed angles $0 < \psi_1 < \pi/2$ and $-\pi/2 < \psi_2 < 0$. Then, the area enclosed by a curve and boundary decreases with constant speed:*

$$\frac{\partial A(t)}{\partial t} = \psi_2 - \psi_1.$$

Proof Since we have the graph $u(x, t)$, the area is as follows

$$A(t) = \int_{b(t)}^{a(t)} u(x, t) dx.$$

When we differentiate it with respect to time t , the Leibniz integral rule gives that

$$\begin{aligned} \frac{\partial A(t)}{\partial t} &= \int_{a(t)}^{b(t)} \frac{\partial u(x, t)}{\partial t} dx + u(b(t), t) \frac{\partial b(t)}{\partial t} - u(a(t), t) \frac{\partial a(t)}{\partial t} \\ &= \int_{a(t)}^{b(t)} \frac{u(x, t)_{xx}}{1 + u(x, t)_x^2} = \arctan(u(b(t), t)_x) - \arctan(u(a(t), t)_x) \\ &= \psi_2 - \psi_1. \end{aligned}$$

The second equality comes from (5.4). Therefore, this implies that, regardless of the shape of the curve, the area decreases, only depending on contact angles ψ_1 and ψ_2 . If we have a non-convex curve, we decompose the curve as a union of graphs of subarc functions $\alpha(t) \in \gamma(t)$. Thus, we have the following result

$$\frac{\partial A(t)}{\partial t} = \psi_2 - \psi_1. \tag{5.5}$$

We note that a similar result is found in [70]. □

Corollary 1 *If the same area is given, the decrease of the area with contact angles cannot exceed the decrease of the area without contact angle.*

Proof It simply follows by equations (4.4) and (5.5). □

Now, we do numerical tests for the curve-shortening flow in the same contact angles and different angles, respectively. In the first case, we consider the evolution of curves with the same contact angles and area, which is enclosed by the curve and boundary, (see Figure 15(a)). Let γ be the non-convex curve consisting of an arc of the circle and line segments that has the same area as enclosed convex curve’s area. If we assume that the arc is the portion of the circle with radius $r_1 = 1$, and line segments passing through the centre $(2, \sqrt{2})$ of the circle with contact angles $\psi_1 = \pi/4$ and $\psi_2 = -\pi/4$, then the distance functions are given by

$$\begin{aligned} d_1(x, y, 0) &= r_1 - \sqrt{(x - 2)^2 + (y - \sqrt{2})^2}, \\ d_2(x, y, 0) &= x - y - 4 + \sqrt{2}, \\ d_3(x, y, 0) &= -x - y + 4 + \sqrt{2}, \end{aligned}$$

and the union of two line segments is

$$d_4(x, y, 0) = \begin{cases} d_1(x, y, 0) & \text{if } d_1(x, y, 0) < d_2(x, y, 0), \\ d_2(x, y, 0) & \text{otherwise.} \end{cases}$$

Then, we have the initial condition,

$$\phi(x, y, 0) = \tanh(d_3(x, y, 0)/\sqrt{2}\epsilon_6) + \tanh(d_4(x, y, 0)/\sqrt{2}\epsilon_6) + 1,$$

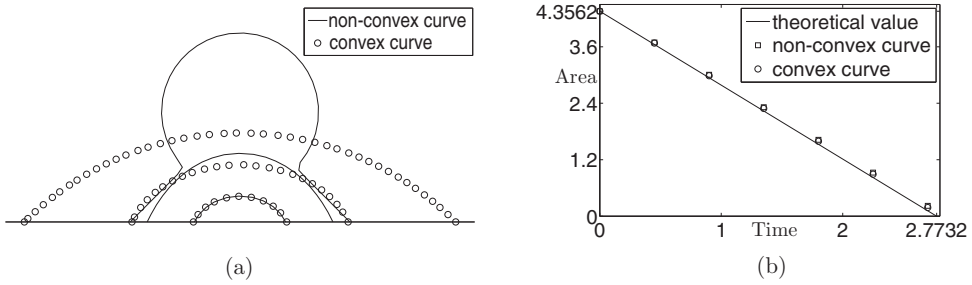


FIGURE 15. (a) non-convex curve the same area and (b) convex curve the same area.

if $\phi(x, y, 0) > 1$, we set $\phi(x, y, 0) = 1$. The initial condition for a convex curve, we set a sector of the circle with radius r_2 to equal the previous one. Thus, we have the following equation

$$2 + \frac{3\pi}{4} r_1^2 = r_2^2 \left(\frac{\pi}{4} - \frac{1}{2} \right).$$

Since $r_1 = 1$, the radius r_2 is to be $\sqrt{(2 + 0.75\pi)/(0.25\pi - 0.5)}$, and the centre is at $(0, -\sqrt{0.5r_2^2})$. The initial condition is given by

$$\phi(x, y, 0) = \tanh \left(\left(r - \sqrt{(x - 4)^2 + (y + \sqrt{0.5r^2})^2} \right) / \sqrt{2}\epsilon_6 \right).$$

In the second case, we evolve the curves having the same area but different contact angles. Let $\psi_1 = 5\pi/6$ and $\psi_2 = -5\pi/6$ be contact angles conditions for the arc of the radius r_1 . We also give contact angle boundary conditions $\psi_1 = \pi/4$ and $\psi_2 = -\pi/4$ for the arc of the circle r_2 . The evolution of curves is shown in Figure 16. Note that the area of two segments enclosed by the curve and boundary is satisfied with the following condition:

$$r_1^2 \left(\frac{2\pi}{3} + \frac{\sqrt{3}}{4} \right) = r_2^2 \left(\frac{\pi}{4} - \frac{1}{2} \right).$$

For simulation, we set $r_1 = 1$ and $r_2 = \sqrt{(2\pi/3 + \sqrt{3}/4)/(\pi/4 - 1/2)}$. The centres of circles are given by $(4, 0.5)$ and $(4, -\sqrt{0.5r_2^2})$, respectively. Thus, the initial condition for the arc of r_1 is given by

$$\phi(x, y, 0) = \tanh \left[\left(r_1 - \sqrt{(x - 4)^2 + (y - 0.5)^2} \right) / \sqrt{2}\epsilon_6 \right],$$

and the initial condition for the arc of r_2 is to be

$$\phi(x, y, 0) = \tanh \left[\left(r_2 - \sqrt{(x - 4)^2 + (y + \sqrt{0.5r_2^2})^2} \right) / \sqrt{2}\epsilon_6 \right].$$

Therefore, area decreases at constant rate, and the rate only depends on contact angles as shown in Figures 15 and 16.

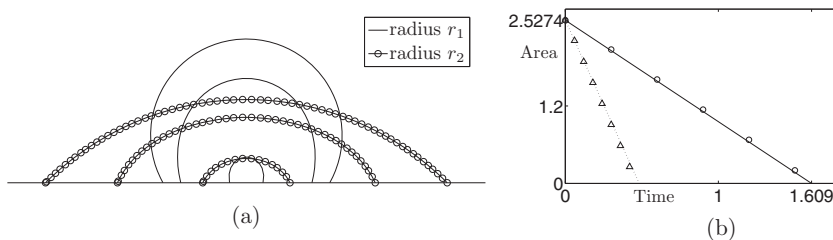


FIGURE 16. Plot (a) indicates that the evolution of curves. The two curves have the same area but different contact angles $\psi_1 = \pi/4$, $\psi_2 = -\pi/4$ and $\psi_1 = 5\pi/6$, $\psi_2 = -5\pi/6$, respectively. (b) Time evolution of the area. Solid and dotted lines are theoretical values of the arc of a circle with radius r_1 and r_2 . Circle and triangle symbols are numerical values of the area of the arcs.

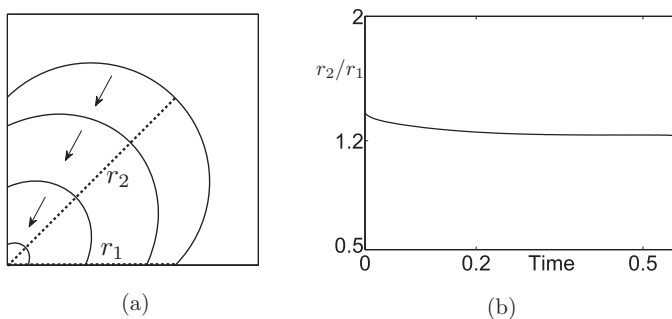


FIGURE 17. (a) self-similar solution and (b) the evolution of r_2/r_1 ratio up to the final time.

5.5 Self-similar solution

Theorem 5.4 (Self-similarity [13, 53, 59, 70]) *Let u satisfy equation (5.4) in the first quadrant, (see Figure 17). Then, there is a unique self-similar solution as $t \rightarrow \infty$.*

Proof In this case, the curve-shortening flow with prescribed angles on the boundary of the first quadrant is considered. If we introduce similarity change of variables $U(\xi, \tau)$ and $\alpha(\tau)$:

$$u(x, t) = \sqrt{2t + 1}U(\xi, \tau), \quad a(t) = \sqrt{2t + 1}\alpha(\tau),$$

where $\xi = x/\sqrt{2t + 1}$ and $\tau = 0.5 \log(2t + 1)$, then we can reformulate the curve-shortening flow equation for a self-similar solution as follows:

$$\begin{aligned} (\arctan(U_\xi))_\xi + \xi U_\xi - U &= 0, \quad x \in (p, 0), \\ U_\xi(p) &= \tan \psi_1, \\ U_\xi(0) &= \tan \psi_2, \\ U(p) &= 0. \end{aligned}$$

Then, the solution converges to the self-similar solution as $t \rightarrow \infty$. □

Here, we examine the self-similar solution with prescribed contact angles. For the initial condition, an arc of the unit circle in the first quadrant is considered. We place its centre at $(0.5, 0.5)$. The distances r_1 and r_2 are defined as the maximum and minimum lengths from the arc to the origin, respectively. For simulation, we take ϵ_6 , $\Delta t = 1.58 \times 10^{-6}$ and $h = 1/256$ in unit square domain $\Omega = (0, 1.5) \times (0, 1.5)$. The simulation is run up until it shrinks to a point. Figure 17(a) shows the self-similar solutions, and (b) illustrates the ratio r_2/r_1 as $t \rightarrow \infty$.

6 Conclusions

We have presented the mechanism of the geometric evolutions using the AC equation with and without contact angles. It is known that the AC equation leads to limiting dynamics in which the interface evolves by the mean curvature flow. In this paper, we considered the behaviour of interface by the mean curvature flow, and then we performed numerical tests to match the geometrical aspects with the limiting solution from the AC problem. Shrinking to a point, avoidance principle, preserving convexity and self-similar solutions were demonstrated for the AC equation with and without contact angles. The results demonstrated that the AC equation is promising in the numerical simulation as well as a theoretical part with contact angles.

Acknowledgement

The corresponding author (J.S. Kim) was supported by the National Research Foundation of Korea (NRF) grant funded by the Korea government (MSIP) (NRF-2014R1A2A2A01003683). This research was also supported partly by the National Research Foundation of Korea (NRF) funded by the Korea government (MSIP) (NRF-2014R1A1A1002667). The authors are grateful to the anonymous referees whose valuable suggestions and comments significantly improved the quality of this paper.

References

- [1] ALLEN, S. M. & CAHN, J. W. (1979) A microscopic theory for antiphase boundary motion and its application to antiphase domain coarsening. *Acta Metall.* **27**(6), 1085–1095.
- [2] ANDREWS, B. & BAKER, C. (2010) Mean curvature flow of pinched submanifolds to spheres. *J. Differ. Geom.* **85**(3), 357–395.
- [3] ANGENENT, S. & GURTIN, M. E. (1989) Multiphase thermomechanics with interfacial structure 2. Evolution of an isothermal interface. *Arch. Ration. Mech. Anal.* **108**(3), 323–391.
- [4] AREZZO, C. & SUN, J. (2013) Self-shrinkers for the mean curvature flow in arbitrary codimension. *Math. Z.* **274**, 993–1027.
- [5] ALTSCHULER, S. J. & WU, L. F. (1993) Convergence to translating solutions for a class of quasilinear parabolic boundary problems. *Math. Ann.* **295**(1), 761–765.
- [6] ALTSCHULER, S. J. & WU, L. F. (1994) Translating surfaces of the non-parametric mean curvature flow with prescribed contact angle. *Calc. Var.* **2**(1), 101–111.
- [7] BARLES, G., BITON, S. & LEY, O. (2002) A geometrical approach to the study of unbounded solutions of quasilinear parabolic equations. *Arch. Ration. Mech. Anal.* **162**, 287–325.
- [8] BARLES, G., SONER, H. M. & SOUGANIDIS, P. E. (1993) Front propagation and phase field theory. *SIAM J. Control. Optim.* **31**(2), 439–469.

- [9] BARRETT, J. W., GARCKE, H. & NÜRNBERG, R. (2010) Parametric approximation of surface clusters driven by isotropic and anisotropic surface energies. *Interface Free Bound.* **12**, 187–234.
- [10] BARRETT, J. W., GARCKE, H. & NÜRNBERG, R. (2010) Finite-element approximation of coupled surface and grain boundary motion with applications to thermal grooving and sintering. *Eur. J. Appl. Math.* **21**, 519–556.
- [11] BARRETT, J. W., GARCKE, H. & NÜRNBERG, R. (2011) The approximation of planar curve evolutions by stable fully implicit finite element schemes that equidistribute. *Numer. Methods Part. D. E.* **27**, 1–30.
- [12] BARTELS, S & MÜLLER, R (2010) Quasi-optimal and robust a posteriori error estimates in $L^\infty(L^2)$ for the approximation of Allen–Cahn equations past singularities. *Math. Comput.* **80**(274), 761–780.
- [13] BELLETTINI, G. & NOVAGA M. (2011) Curvature evolution of nonconvex lens-shaped domains. *J. Reine Angew. Math.* **2011**, 17–46.
- [14] BENEŠ, M. (2003) Diffuse-interface treatment of the anisotropic mean-curvature flow. *Appl. Math.* **48**(6), 437–453.
- [15] BOBENKO, A. I. & SPRINGBORN, B. A. (2007) A discrete Laplace–Beltrami operator for simplicial surfaces. *Discrete Comput. Geom.* **38**(4), 740–756.
- [16] BRAKKE, K. (1978) *The Motion of a Surface by its Mean Curvature*, Math Notes, Princeton University Press, Princeton, New York.
- [17] BRONSARD, L. & KOHN, R. V. (1991) Motion by mean curvature as the singular limit of Ginzburg–Landau dynamics. *J. Differ. Eq.* **90**(2), 211–237.
- [18] CAGINALP, G. & CHEN, X. (1998) Convergence of the phase field model to its sharp interface limits. *Eur. J. Appl. Math.* **9**, 417–445.
- [19] CAO, H. D. & LI, H. (2013) A gap theorem for self-shrinkers of the mean curvature flow in arbitrary codimension. *Calc. Var.* **46**, 879–889.
- [20] CHEN X. (1994) Spectrum for the Allen–Cahn, Cahn–Hilliard, and phase-field equations for generic interfaces. *Commun. Part. Differ. Eq.* **19**(7–8), 1371–1395.
- [21] CHEN, Y. G., GIGA, Y. & GOTO S. (1991) Uniqueness and existence of viscosity solutions of generalized mean curvature flow equations. *J. Differ. Geom.* **33**, 749–786.
- [22] CHEN, X. & GUO J. S. (2011) Motion by curvature of planar curves with end points moving freely on a line. *Math. Ann.* **350**(2), 277–311.
- [23] CHOPP, D. L. (1993) Computing minimal surfaces via level set curvature. *J. Comput. Phys.* **106**, 79–91.
- [24] CHOPP, D. L. (1994) Computation of self-similar solutions for mean curvature flow. *Exp. Math.* **3**(2), 1–15.
- [25] CHOPP D. L. & SETHIAN J. A. (1993) Flow under curvature: singularity formation, minimal surfaces, and geodesics. *Exp. Math.* **2**(4), 235–255.
- [26] DECKELNICK, K., DZIUK, G. & ELLIOTT, C. M. (2005) Computation of geometric partial differential equations and mean curvature flow. *Acta Numer.* **14**, 139–232.
- [27] DIRR, N., KARALI, G. & YIP, N. K. (2008) Pulsating wave for mean curvature flow in inhomogeneous medium. *Eur. J. Appl. Math.* **19**, 661–699.
- [28] DZIUK, G. & ELLIOTT, C. M. (2012) L^2 - estimates for the evolving surface finite element method. *Math. Comput.* **82**(281), 1–24.
- [29] ECKER K. (2004) *Progress in Nonlinear Differential Equations and their Applications, Regularity Theory for Mean Curvature Flow*, Birkhäuser, Boston.
- [30] ELSEY, M. & ESEDOĞLU, S. (2009) Analogue of the total variation denoising model in the context of geometry processing. *Multiscale Model. Simul.* **7**(4), 1549–1573.

- [31] EPSTEIN, C. L. & GAGE, M. (1987) *The Curve Shortening Flow. Wave Motion: Theory, Modelling, and Computation*, Springer, New York.
- [32] EVANS, L. C., SONER, H. M. & SOUGANIDIS, P. E. (1992) Phase transitions and generalized motion by mean curvature. *Commun. Pure Appl. Math.* **45**(9), 1097–1123.
- [33] EVANS, L. C. & SPRUCK, J. (1991) Motion of level sets by mean curvature I. *J. Differ. Geom.* **33**(3), 635–681.
- [34] EVANS L. C. & SPRUCK, J. (1992) Motion of level sets by mean curvature II. *Trans. Am. Math. Soc.* **1**(1), 321–332.
- [35] EVANS L. C. & SPRUCK, J. (1992) Motion of level sets by mean curvature III. *J. Geom. Anal.* **2**(2), 121–150.
- [36] EVANS L. C. & SPRUCK, J. (1995) Motion of level sets by mean curvature IV. *J. Geom. Anal.* **1**(1), 77–114.
- [37] FENG, X., HE Y. & LIU C. (2006) Analysis of finite element approximations of a phase field model for two-phase fluids. *Math. Comput.* **76**(258), 539–571.
- [38] FENG X. & PROHL, A. (2003) Analysis of a fully discrete finite element method for the phase field model and approximation of its sharp interface limits. *Math. Comput.* **73**(246), 541–567.
- [39] FENG, X. & WU, H. J. (2005) A posteriori error estimates and an adaptive finite element method for the Allen–Cahn equation and the mean curvature flow. *J. Sci. Comput.* **24**(2), 121–146.
- [40] GAGE, M. & HAMILTON, R. S. (1986) The heat equation shrinking convex plane curves. *J. Differ. Geom.* **23**(1), 69–96.
- [41] GHOUSSEUB, N. & GUI, C. (2003) On De Giorgi’s conjecture in dimensions 4 and 5. *Ann. Math.* **157**(1), 313–334.
- [42] GRAYSON, M. A. (1987) The heat equation shrinks embedded plane curves to points. *J. Differ. Geom.* **26**(2), 285–314.
- [43] Grayson, M. A. (1989) A short note on the evolution of a surface by its mean curvature. *Duke Math. J.* **58**(3), 555–558.
- [44] Grayson M. A. (1989) Shortening embedded curves. *Ann. Math.* **129**(1), 71–111.
- [45] GUGGENHEIMER, H. W. (1977) *Differential Geometry*, Dover Publications, New York.
- [46] GURTIN, M. E. (1988) Multiphase thermomechanics with interfacial structure 1. Heat conduction and the capillary balance law. *Arch. Ration. Mech. Anal.* **104**(3), 195–221.
- [47] HANDLOVIČOVÁ, A. & MIKULA, K. (2008) Stability and consistency of the semi-implicit co-volume scheme for regularized mean curvature flow equation in level set formulation. *Appl. Math.* **53**(2), 105–129.
- [48] HEINEMANN, C. & KRAUS, C. (2013) Existence results for diffuse interface models describing phase separation and damage. *Eur. J. Appl. Math.* **24**, 179–211.
- [49] HUISKEN, G. (1984) Flow by mean curvature of convex surfaces into spheres. *J. Differ. Geom.* **20**(1), 237–266.
- [50] HUISKEN, G. (1998) A distance comparison principle for evolving curves. *Asian J. Math.* **2**(1), 127–134.
- [51] HUISKEN, G. (1989) Non-parametric mean curvature evolution with boundary conditions. *J. Differ. Equ.* **77**(2), 369–378.
- [52] ILMANEN, T. (1993) Convergence of the Allen–Cahn equation to Brakke’s motion by mean curvature. *J. Differ. Geom.* **38**(2), 417–461.
- [53] KOHSAKA, Y. (2001) Free boundary problem for quasilinear parabolic equation with fixed angle of contact to a boundary. *Nonlinear Anal.* **45**(7), 865–894.
- [54] LADYENSKAJA, O. A., SOLONNIKOV, V. A. & URAL’CEVA N. N. (1968) Linear and quasilinear equations of parabolic type. *Am. Math. Soc.* **23**.
- [55] LEE, H.-G. & KIM J. (2011) Accurate contact angle boundary conditions for the Cahn–Hilliard equations. *Comput. Fluids* **44**(1), 178–168.
- [56] LI, Y., LEE, H.-G., JEONG, D. & KIM, J. (2010) An unconditionally stable hybrid numerical method for solving the Allen–Cahn equation. *Comput. Math. Appl.* **60**(6), 1591–1606.

- [57] LIE, J., LYSAKER, M. & TAI, X-C. (2006) A variant of the level set method and applications to image segmentation. *Math. Comput.* **75**(255), 1155–1174.
- [58] MANTEGAZZA, C. (2011) Lecture notes on mean curvature flow, volume 290 of Progress in Mathematics. Birkhauser/Springer Basel AG, Basel.
- [59] MANTEGAZZA, C., NOVAGA, M. & TORTORELLI, V. N. (2004) Motion by curvature of planar networks. *Ann. Scuola Norm. Sup. Pisa Cl. Sci. (5)* **3**, 235–324.
- [60] MERRIMAN B., BENCE, J. & OSHER, S. (1992) Diffusion-generated motion by mean curvature. In: E. Taylor (editor), *Computational Crystal Growers Workshop*, pp. 73–83.
- [61] MOTTONI, P. D. & SCHATZMAN M. (1995) Geometrical evolution of developed interfaces. *Trans. Am. Math. Soc.* **347**(5), 1533–1589.
- [62] Mullins, W. W. (1956) Two-dimensional motion of idealized grain boundaries. *J. Appl. Phys.* **27**, 900–904.
- [63] PAN, Z. & WETTON, B. (2008) A numerical method for coupled surface and grain boundary motion. *Eur. J. Appl. Math.* **19**, 311–327.
- [64] PINO, M., KOWALCZYK, M. & WEI, J. (2011) On De Giorgi’s conjecture in dimension $N \geq 9$. *Ann. Math.* **174**(3), 1485–1569.
- [65] Press W. H., Teukolsky S. A., Vetterling W. T., and Flannery B. P. (2002) *Numerical Recipes in C++*, 2nd ed., Cambridge University, Cambridge.
- [66] REN, X. & WEI, J. (2009) On a phase-field problem driven by interface area and interface curvature. *Eur. J. Appl. Math.* **20**, 531–556.
- [67] RUBINSTEIN, J., STERNBERG, P. & KELLER, J. B. (1989) Fast reaction, slow diffusion, and curve shortening. *SIAM J. Appl. Math.* **49**(1), 116–133.
- [68] RUUTH, S. (1998) Efficient algorithms for diffusion-generated motion by mean curvature. *J. Comput. Phys.* **144**, 603–625.
- [69] SAPIRO, G. (2006) *Geometric Partial Differential Equations and Image Analysis*, Cambridge University, Cambridge.
- [70] SCHNÄRER, O. C., AZOUANI, A., GEORGI, M., HELL, J., JANGLE, N., KOELLER, A., MARXEN, T., RITTHALER, S., SÁEZ, M., SCHULZE, F. & SMITH, B. (2011) Evolution of convex lens-shaped networks under the curve shortening flow. *Trans. Am. Math. Soc.* **363**(5), 2265–2294.
- [71] SMOCZYK, K. (2012) *Global Differential Geometry: Mean Curvature Flow in Higher Codimension: Introduction and Survey*, Springer, Berlin Heidelberg.
- [72] SONER, H. M. (1993) Motion of a set by the curvature of its boundary. *J. Differ. Equ.* **101** 313–372.
- [73] SONER, H. M. (1997) Ginzburg–Landau equation and motion by mean curvature, I: Convergence. *J. Geom. Anal.* **7**(3), 437–475.
- [74] SONER, H. M. (1997) Ginzburg–Landau equation and motion by mean curvature, II: Development of the initial interface. *J. Geom. Anal.* **7**(3), 477–491.
- [75] TSO, K. (1985) Deforming a hypersurface by its Gauss-Kronecker curvature. *Commun. Pure Appl. Math.* **38**(6), 867–882.
- [76] ZHU, X.-P. (2002) Studies in Advanced Mathematics, *Lectures on Mean Curvature Flows*, AMS, International Press, Somerville.
- [77] XU, G. (2004) Surface fairing and featuring by mean curvature motions. *J. Comput. Appl. Math.* **163**, 295–309.